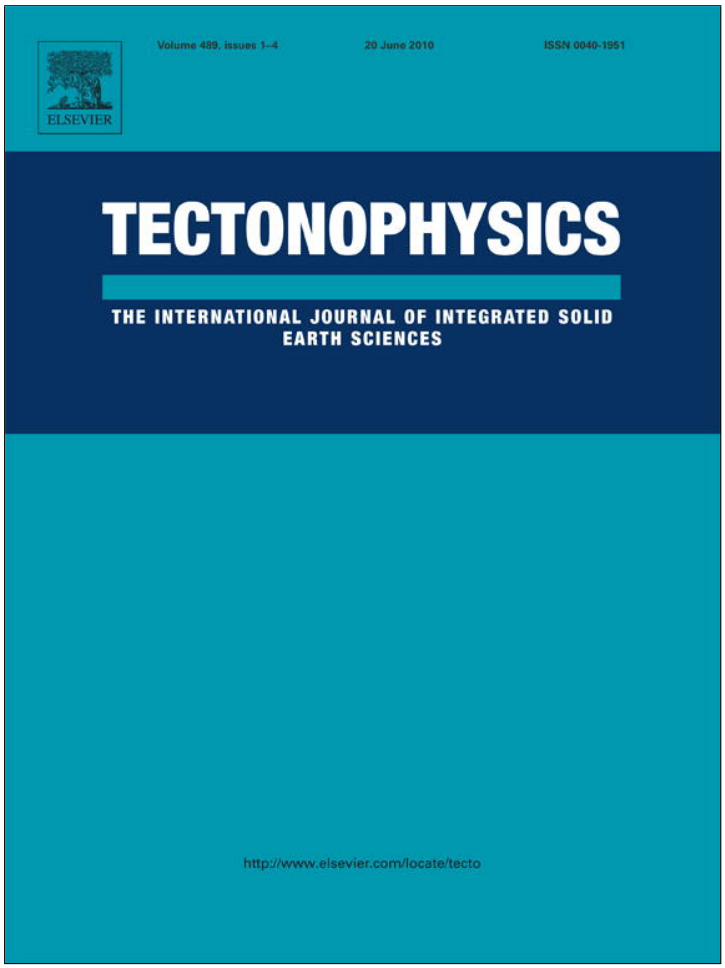

Tectonophysics 489 (2010) 240–247

Contents lists available at ScienceDirect

Tectonophysics

journal homepage: www.elsevier.com/locate/tecto

Pre-seismic geomagnetic anomaly and earthquake location

Chieh-Hung Chen [a,b], Jann-Yenq Liu [b,c,*], Pei-Ying Lin [d], Horng-Yuan Yen [e], Katsumi Hattori [f], Wen-Tzong Liang [a], Yuh-Ing Chen [g], Yih-Hsiung Yeh [a], Xiaoping Zeng [h]

[a] Institute of Earth Sciences, Academia Sinica, Taipei 115, Taiwan
[b] Institute of Space Science, National Central University, Chung-Li 32054, Taiwan
[c] Center for Space and Remote Sensing Research, National Central University, Chung-Li 32054, Taiwan
[d] School of Earth and Space Exploration, Arizona State University, Tempe AZ 85287, USA
[e] Institute of Geophysics, National Central University, Chung-Li 32054, Taiwan
[f] Marine Biosystems Research Center, Chiba University, Inage, Chiba 263-8522, Japan
[g] Institute of Statistics, National Central University, Chung-Li 32054, Taiwan
[h] Institute of Geophysics, China Seismological Bureau, Beijing 100081, China

ARTICLE INFO

Article history:
Received 24 March 2008
Received in revised form 6 April 2010
Accepted 19 April 2010
Available online 24 April 2010

Keywords:
Geomagnetic field
Focal mechanism
Earthquake forecast

ABSTRACT

Many researchers studied the relationships between appearances of geomagnetic anomalies and their distances to earthquake epicenters or faults. Yet, occasionally some magnetometer stations located nearby earthquake epicenters and/or faults do not observe geomagnetic anomalies. In this paper, a new hybrid system which simultaneously takes the hypocenter and fault plane solution into account is constructed to examine 38 earthquakes interpreted to be associated with geomagnetic anomalies during the period 1988–2001 in Taiwan. The Surface Magnetic Anomaly Reference Tip (SMART) of the new system is used instead of the epicenter or the fault to investigate statistically the distance relationship between the anomalies and the earthquake parameters. Results show that the anomalies gather along the fault and in the belt zone to the SMART. Possible mechanisms causing the anomalies in the two zones are proposed and discussed. Characteristics of the anomaly might shed some light on locations of faults before earthquake occurrences.

1. Introduction

Geomagnetic anomalies associated with major earthquakes have been reported by many scientists (see papers listed in Fraser-Smith et al., 1990; Hayakawa and Fujinawa, 1994; Hayakawa, 1999; Hayakawa and Molchanov, 2002; Chen et al., 2004; Zeng et al., 2002; and Liu et al., 2006). They suggest that appearances of geomagnetic anomalies of an earthquake are related to its magnitude and the epicentral distance. Hattori (2004) found that pre-earthquake anomalies were often observed by magnetometers close to earthquake epicenters. However, sometimes no anomalies associated with earthquakes are observed even where magnetometers are set nearby epicenters.

When an earthquake is associated with a surface rupture or an exposed fault, it is best the chance to observe the relative position between the fault and the epicenter. Since a hypocenter usually is not right under the associated surface rupture, the epicenter could be very far away from the exposed fault. For example, the distance between the epicenter and the fault of the M7.3, September 20, 1999 Chi-Chi earthquake is about 10 km (Chen et al., 2001). Thus, the earthquake fault (the fault system) instead of the epicenter becomes the reference for studying the geomagnetic anomalies (for example, Yen et al., 2004). Note that a fault is generally considered as a place where stress is accumulated. Merzer and Klemperer (1997) suggest that geomagnetic anomalies are caused by induced electric currents flowing in the fault zone during the earthquake preparation period. Although, Yen et al. (2004) observe that the pre-earthquake anomaly strength is related to distances between magnetic stations and the earthquake fault, similar to taking the epicenter as a reference/coordinate system, sometimes magnetometers located near faults might also fail to register any geomagnetic anomalies before large earthquakes. For example, Bakun et al. (2005) and Langbein (2005) report that no geomagnetic anomalies are observed during the 2004/9/28 Parkfield earthquake, even when magnetometers are just set nearby the San-Andreas fault.

Both successes and failures in recordings suggest that the epicenter and fault reference systems need be taken into account. In this paper, we construct a new reference system by simultaneously taking the epicenter and fault into account to examine the relationship between geomagnetic anomalies and $M \geq 5.0$ earthquakes, which occurred in Taiwan during 1988–2001 (Fig. 1).

2. Theory and methodology

Chapman and Bartels (1940) found that geomagnetic daily variations recorded by magnetometers were influenced by current

* Corresponding author. Institute of Space Science, National Central University, Chung-Li 32054, Taiwan. Tel.: +886 3 4228374; fax: +886 3 4224394.
E-mail address: jyliu@jupiter.ss.ncu.edu.tw (J.-Y. Liu).

0040-1951/$ – see front matter
doi:10.1016/j.tecto.2010.04.018

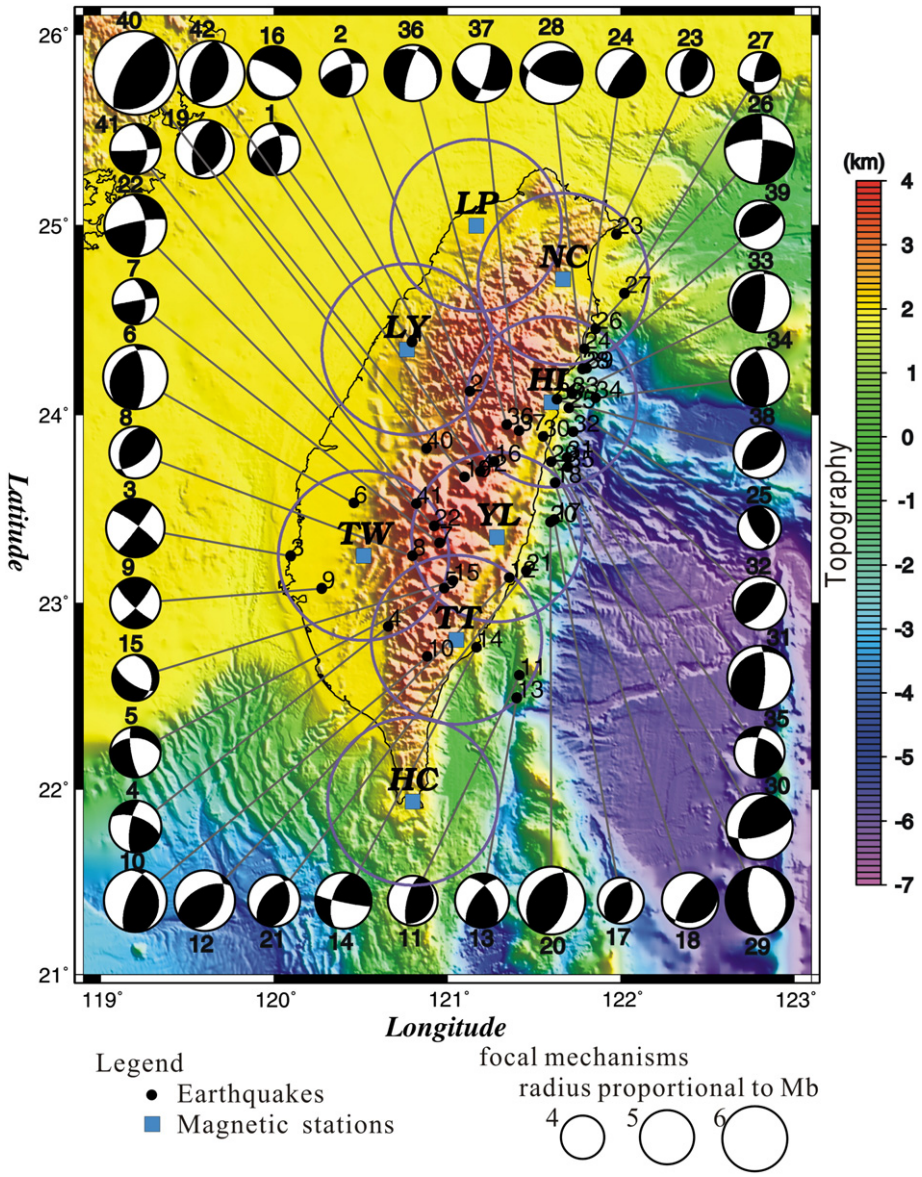

Fig. 1. The hypocenters and focal mechanisms of 38 earthquakes ($M \geq 5.0$) and the eight magnetometer stations from 1988 to 2001. The subduction of the Southern China Sea plate beneath the Philippine Sea plate and the Philippine Sea plate beneath the Eurasian plate in eastern Taiwan causes many large earthquakes to occur with complex focal mechanisms and deep depths. However, thrust fault earthquakes with shallow depths have caused much loss of life in western Taiwan. The purple circles denote the radii of 50 km from the magnetometers.

and/or field changes in the ionosphere, magnetosphere, and the inducting field. Changes of the solar wind, ionosphere and magnetosphere properties simultaneously affecting the whole Earth are considered to be primary effects that occur on a global scale. Moreover, induction of secondary fields is generated on both global and local scales. Induction on a local scale can be observed by the geomagnetic depth sounding technique (Prasad et al., 1993; Prasad, 1999; Liu et al., 2006). The technique utilizes the natural frequency variation of the geomagnetic field caused by the solar wind.

To discriminate primary and/or globe effects from secondary and/or local effects, a network of magnetometers is required and employed (Fig. 1 and Table 1). One setup in a low seismicity area is taken as a reference station and the other located in a seismically active place is used as a monitored station. In fact, globe effects are almost the same at two nearby stations. Therefore, when underground rocks or conductivity remain unchanged, the ratios of geomagnetic daily variations between the reference and monitored stations mainly show the difference of the geomagnetic latitude and geology at those two sites. By contrast, when stressed rocks near the monitored station produce electric current and/or change the geology underground, the ratio between two station changes accordingly and the anomalies included in the induction field can be observed (Liu et al. 2006).

In this paper, the anomalies given by subtracting the minimum from the maximum of the geomagnetic field are used to understand the variations underground. For example, Fig. 2 displays the daily

Table 1
Locations of magnetometer stations.

Station	Latitude (°N)	Longitude (°E)
Lunping (LP)	25.0	121.2
Neicheng (NC)	24.7	121.6
Liyutan (LY)	24.3	120.8
Hualien (HL)	24.1	121.6
Yuli (YL)	23.4	121.3
Tsengwen (TW)	23.3	120.5
Taitung (TT)	22.8	121.0
Hengchun (HC)	21.9	120.8

maximum BM_{LP} (BM_{LY}), minimum Bm_{LP} (Bm_{LY}) and their associated range $\Delta B_R = BM_{LP} - Bm_{LP}$ ($\Delta B_O = BM_{LY} - Bm_{LY}$) of the geomagnetic total field (Chapman and Bartels, 1940) observed at LP (LY) station. For nearby reference (LP) and monitored stations (LY, TW, TT, YL, HL and NC), the ratio, Rro ($=\Delta B_R/\Delta B_O$,) and/or Ror ($=\Delta B_O/\Delta B_R$,) is approximately equal to 1. Note that the ratio may be slightly greater or less than 1, which depends mainly on the relative geomagnetic latitudes of the two stations. For symmetry, we compute the ratios of Rro for $\Delta B_R \leq \Delta B_O$ and Ror for $\Delta B_R \geq \Delta B_O$. By contrast, when stressed rocks produce electric current as well as the electrical and/or magnetic property changes during the earthquake preparation period, the daily range ratios between reference and monitored stations might become greater or less than the normal mean value (Liu et al., 2006). To detect anomalous signatures, we construct the background distribution from the entire 13-year and the observed distribution from a moving 31-day window of the ratio Rro for each monitored station (also see, Liu et al., 2006). The difference between two distribution peaks is denoted the anomaly strength.

To construct a new reference system for suitably studying pre-earthquake geomagnetic anomalies, the nodal planes obtained from the fault plane solutions whose strikes, dips, and slips involved by focal mechanisms, as well as the relocation earthquake data (Engdahl et al., 1998) are taken into account. The slip plane of the nodal planes is named the fault plane and the other orthogonal one is called the auxiliary fault plane (Shearer, 1999). Here, for an earthquake without a surface rupture, the fault and the auxiliary fault planes are determined by the earthquake's aftershocks. These two planes intersecting any horizontal plane form the fault and the auxiliary fault lines with their strike directions. Therefore, the two lines cross on the hypocenter at the earthquake's depth (Fig. 3). In fact, the epicenter system is the two lines vertically projecting onto the Earth's surface with the epicenter as one reference, while the fault system takes the fault plane intersecting the Earth's surface, i.e. the surface rupture, as the other reference. By combining the essence of the two, a new coordinate system is constructed by projecting the two lines respectively with both the fault and auxiliary fault planes onto the Earth's surface (the hybrid system). Note that the origin of the hybrid system, Surface Magnetic Anomaly Reference Tip (SMART) point (or distance reference point), is at the end point of the intersection line of the two extended planes on the Earth's surface, and the two surface reference axes are the fault and auxiliary fault lines projected with an

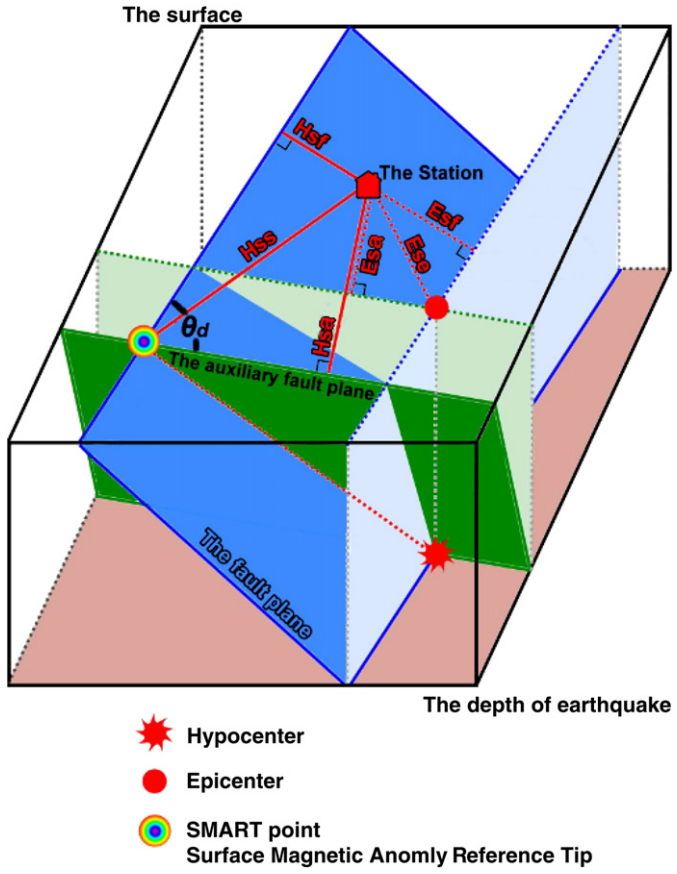

Fig. 3. The planned distribution of the two planes during an earthquake. The dashed line indicates the intersection of the fault and auxiliary fault planes; the hypocenter (red sun) and SMART (rainbow circle) point indicate the depth of the earthquake and the intersection on the line drawn through the surface, respectively. The red circle denotes the epicenter on the surface. Notably, regarding to the fault system, the anomalies are related with the distance from the stations to the fault line on the surface (Hsf). Ese, Esf and Esa are correlated to determine the position in the epicenter system and Hss, Hsf and Hsa denote the three different distances from the station of the two planes in the hybrid system. An angle, θ_d, is determined between the fault and auxiliary fault lines on the surface.

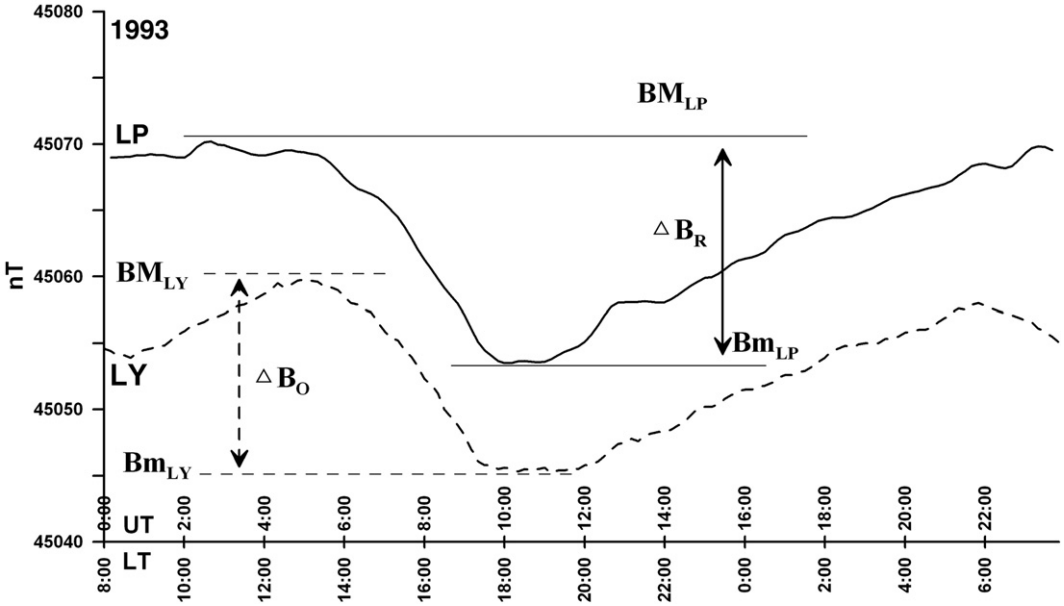

Fig. 2. The average curves of daily variations recorded at the LP (solid line) and LY (dashed line, shifted by 400 nT) stations in 1993. For example, the associated range of ΔB_R and ΔB_O are 17.2 and 14.6 nT, respectively. In this example, the average ratio Rro is 1.18 (=17.2/14.6) and its reciprocal Ror is 0.85 (=14.6/17.2). In practical application, the ratios are daily calculated.

assumption of their constant dips given by the earthquake fault plane solutions. For cross examinations among the epicenter, fault, and hybrid systems, six distances from the geomagnetic monitored station (i.e. geomagnetic anomaly location) to the two origins (Ese and Hss), to the two fault projected lines (Esf and Hsf), and to the two auxiliary fault projected lines (Esa and Hsa) are calculated, respectively.

3. Observation and interpretation

Taiwan offers an excellent opportunity for studying pre-earthquake geomagnetic anomaly phenomena because it is located on the western side of the circum-Pacific seismic zone where the interaction between the Philippine Sea plate and the Eurasian plate is intense and complicated (Wang et al., 2002). To understand complex geological structures and observe geomagnetic total fields, eight magnetometers (with a sensitivity of 0.1 nT, and a sample rate of 10 min) were set up far away from electric power lines, iron rods and buildings in Taiwan (Yen et al., 2004). The locations of every station are listed in Table 1 and the distances between each of them are less than 130 km (Fig. 1). The reference station, Lungping (LP), is located in a low seismicity area, and no large earthquake has occurred within a radius of 50 km from the LP station from 1988 to 2001 (Liu et al., 2006). The Hengchun (HC) station is located in southern Taiwan. Because of the existence of many data gaps at the HC station, the analyses are limited to the other six stations and the reference station.

Let's take the variations of the geomagnetic field at the monitored station LY and the reference station LP before and after the Chi-Chi earthquake as an example to see what happens for the observed distributions (Fig. 4). Fig. 4 shows that the observed distribution, which is similar with the background 5 months before the earthquake (3/31–4/30, 1999, due to a lack of observation data in LY station). The observed distributions in the two periods, 1 month before (8/5–9/4) and during the earthquake occurrence month (9/5–10/5), significantly depart with the anomaly strengths 0.75 and 0.75 from the background. The anomaly strength becomes much small 0.5–1.5 months after the Chi-Chi earthquake. Then, the observed distribution 2 months (11/6–12/6) after the earthquake is generally similar to the background. We also examined the data from the TW station near the Chi-Chi earthquake. Simultaneously, Fig. 5 displays that the observed distribution (9/5–10/5, 1998) at the TW station is similar with the background a long time before the earthquake. The observed distribution significantly departs from the background during the Chi-Chi earthquake and the Chia-Yi earthquake (the 8th event in Fig.1, M6.4, October 22, 1999), and becomes similar to background data

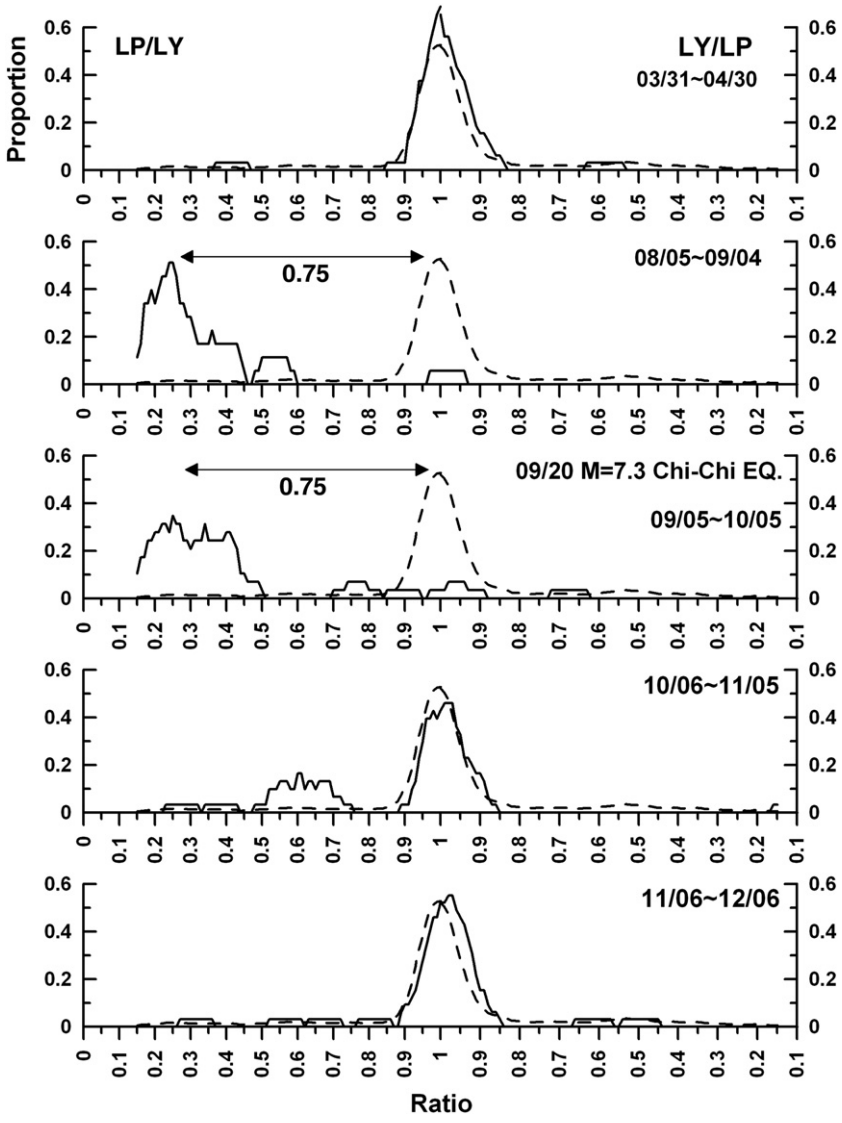

Fig. 4. The observed distributions (solid curves) in five time periods during the Chi-Chi earthquake together with the background distribution (dashed curves) at the LY station in 1999. The vertical axes are the distributions in the number of proportion of the ratios, and the horizontal axes represent the ratios of Rro and Ror.

again 1 month and a half after the last earthquake. Owing to many data gaps at NC during the Chi-Chi earthquake, we compare the observed distributions of the stations (LY and TW) close to and (TT, YL and HL) far away from the event to understand the variations during 9/5 and 10/5 in 1999. Fig. 6 reveals that the observed distribution of TT, YL and HL stations are similar with their background while the two distributions are significantly different in LY and TW. This indicates that the anomalies detected at the two nearby stations, LY and TW, are the internal local effect associated with the Chi-Chi earthquake.

For a statistical study, geomagnetic variations and 38 earthquakes, which are posted with associated focal mechanisms, are examined during the entire 13-year period. The mechanisms of earthquakes are published by the Harvard CMT catalog (http://www.globalcmt.org/CMTsearch.html) and Broadband Array in Taiwan for Seismology (BATS) (Kao et al., 2002; Liang et al., 2003, 2004). Since two earthquakes occurred between two stations and one earthquake appeared among three stations, geomagnetic anomalies associated with $42(=38+1\times2+2\times1)$ earthquake events are examined by using the epicenter, fault and hybrid (or SMART) systems.

Fig. 7 illustrates anomaly appearances at the epicenter (Fig. 7a, d, and f), fault (Fig. 7b), and hybrid systems (Fig. 7c, e, and g). Due to both solid and open circles randomly appearing in a small region, no clear relationship is found between the anomaly appearances and the distances of Esf and Esa in the epicenter system (Fig. 7a). For the fault system, we examine the anomaly proportion and Hsf (Fig. 7b). Fig. 7b shows that the proportion is rather complex and that of Hsf<8 km is 100%, and no anomalies are beyond Hsf = 72 km. By contrast, for the hybrid system, the anomalies mainly occur either in a narrow strip along the fault plane or a belt zone some distance from SMART (Fig. 7c), which implies two possible physical mechanisms being important. Moreover, an angle (θ_d) between the fault and auxiliary fault lines on the surface, where the station is located, is the other parameter to be examined. Fig. 7d reveals that most events spread from 0° to 180° with different Ese and therefore there is no conspicuous relationship between Ese and θ_d. It is interesting to see that the triangle symbols (Hsf<8 km) in Fig. 7c generally appear along the fault line, but surprisingly those in Fig. 7e yield no clear correlation between θ_d and Hss. By contrast, the solid circle symbols in the belt zone of Fig. 7c yield an anomaly ribbon that Hss is inversely proportional to θ_d of Fig. 7e. The open circle symbols near the belt zone of Fig. 7c distribute at the two sides of the anomaly ribbon. In previous studies, the anomaly strength was found reciprocally proportional to Ese (for example, Hattori, 2004). However, Fig. 7f does not display such a correlation and the occurrence proportion of anomalous events maintains at about 75.4%, which is generally considered the observation probability of pre-earthquake anomalous

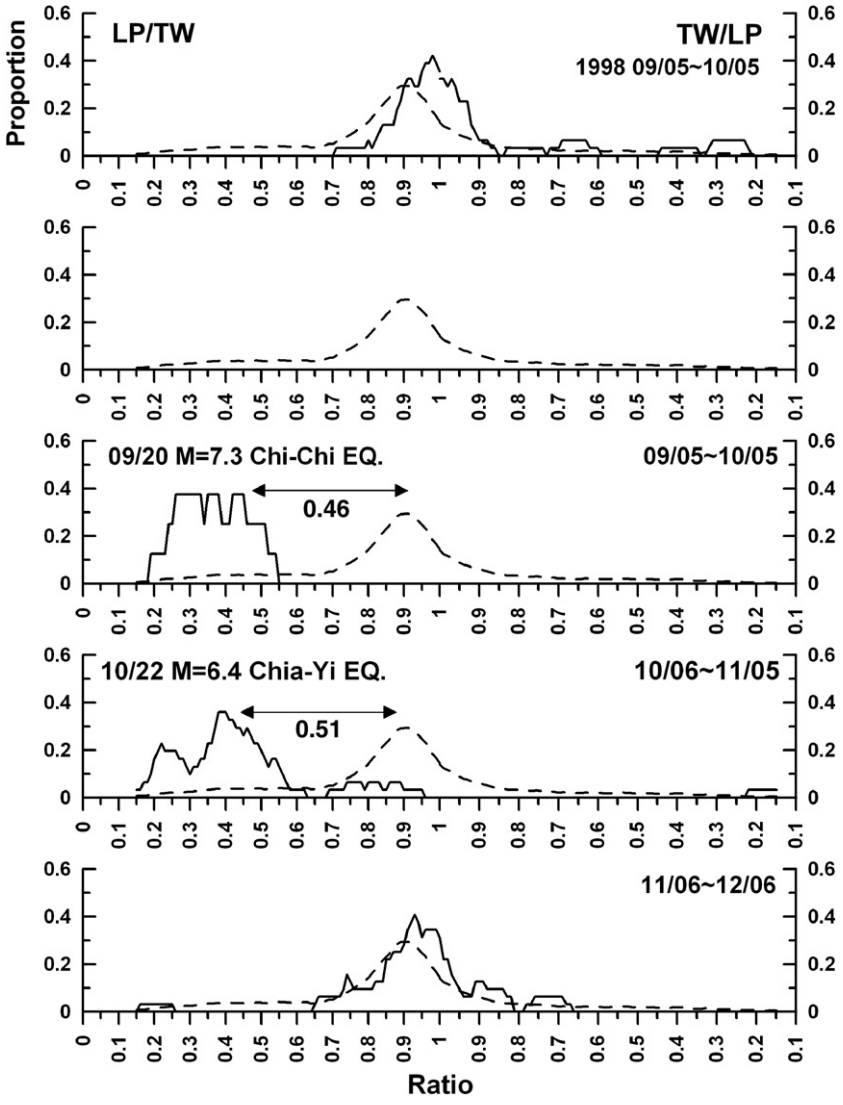

Fig. 5. The observed distributions (solid curves) during five time periods in the Chi-Chi earthquake together with the background distribution (dashed curves) at the TW station in 1999, except the top diagram. Note that the observed distribution is computed with data during 9/5–10/5, 1998, due to a lack of observation data 10/5, 1998–10/27, 1999.

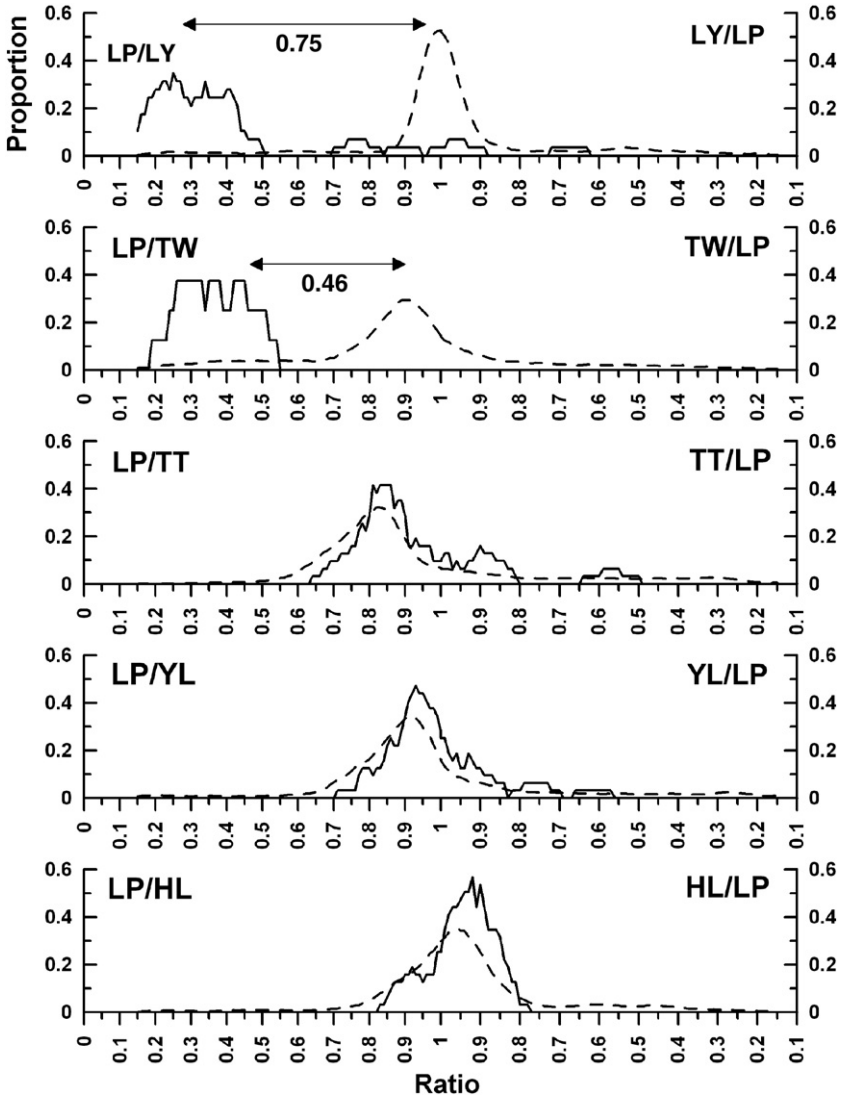

Fig. 6. The observed distributions at each magnetometer station during the month (9/5–10/5, 1999) of the Chi-Chi earthquake. The background and observed distributions are denoted by dashed and solid curves, respectively.

phenomena (Liu et al., 2006). Alternatively, Fig. 7g shows a new anomaly distribution of the events, which are far away from the faults. Most events with the strong anomaly strength and the occurrence proportion of anomalous events both occur within the range of 40 and 60 km in $(Hsf^2 + Hsa^2)^{1/2}$ (Fig. 7 g). Meanwhile, it is clear to find that the boundary of the anomaly strength between the anomalous and failure events is 0.045. If the anomaly strength is greater than 0.045, we can then declare that the pre-earthquake geomagnetic anomaly is observed as an anomaly event. Note that if the range of the daily variation is 40 nT, the boundary of the anomaly strength is about 2 nT.

4. Discussion and conclusion

Fig. 7c displays the geomagnetic anomalies appearing along the fault planes and in the belt zone. This implies that mechanisms of the two zones are different. Many papers infer that anomalies associated with earthquakes are caused by changes of susceptibility and conductivity, which are produced by different mechanisms, such as stressed rock (Stacey, 1962; Nagata, 1970), small conductivity fluctuations (Egbert, 2002) and piezomagnetism (Johnston, 1997; Nishida et al., 2004).

Scientists (Booth et al., 1990; Crampin, 1994; Crampin et al., 1999; Winterstein and Meadows, 1991) observed micro-cracks occurring along the fault plane. Since micro-cracks are a direct evident of stress, rock susceptibilities (Stacey, 1962; Nagata, 1970) have been modified during the earthquake preparation period. Although causal mechanisms are not fully understood, changes of susceptibilities and conductivities (Chen and Chen, 2000) together with associated current could result in the geomagnetic anomalies before the earthquakes. Based on the characteristics of the anomalies along the fault plane (Fig. 7c), the narrow strip through SMART can be employed in determining the slip plane (the fault plane) before earthquake occurrences. Meanwhile, we examine the relationship between the belt zone in Fig. 7c and the associated stress distribution for each earthquake. The earthquake stress distribution usually can be explained by a double couple result, which is a pair of complementary forces producing no net torque; each force couple opposing point forces is separated by a distance (Shearer, 1999). Since the force generally decreases with the distance, the torque approaches zero near the SMART due to the small force and a very short moment arm. This indirectly explains the observations of Chen et al. (2004) and Zeng et al. (2002) that the change rates of the geomagnetic field near epicenters tend to be a small constant before earthquakes. On the other hand, the torque far away from SMART due to a long moment arm and a very small force is also small. It can be seen in the belt zone of Fig. 7c that the torque is large due to the large force with an inter-

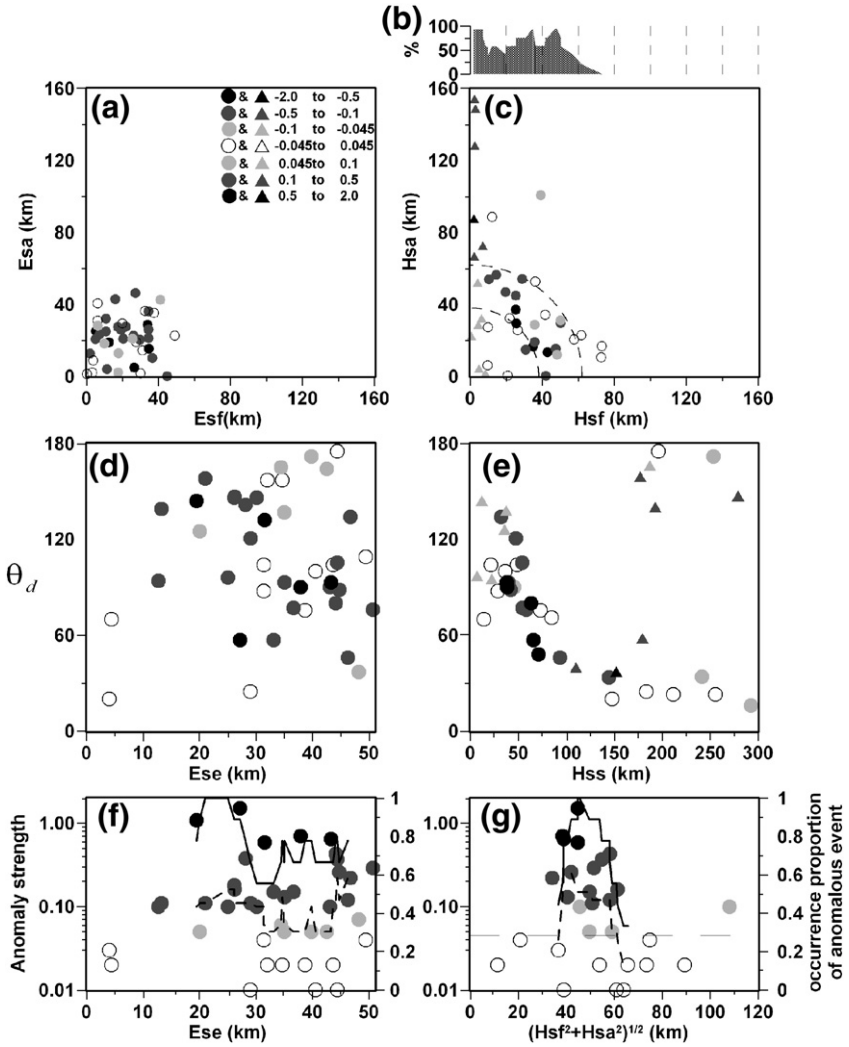

Fig. 7. The relationship between the anomaly distribution and the earthquake parameters in the epicenter, fault and hybrid systems. The panels on the right, (a, d and f) show the relationships in the epicenter system and the circles denote the study events. The proportions reveal anomaly observations to Hsf during earthquakes and the line shows their median with a window of 5 events in the fault system (b). The correlations derived from the hybrid system (c, e and g). The triangles and circles are the study events near and away from the fault lines, respectively. The gray triangles and circles denote the earthquakes with different anomaly strengths. The anomaly distributions relate to the surface distances from station to fault and auxiliary fault planes in the different systems (a and c). The θ_d correlates to the Ese and Hss (d and e). The strength of anomaly varies with the Ese (f), and the same anomaly with $(Hsf^2+Hsa^2)^{1/2}$ (g) are presented. Their solid and dashed lines respectively denote the occurrence proportion of anomalies and median anomaly strength calculated by running windows for the 9 events (f and g). The long dashed line denotes that the anomaly strength equals to 0.045 in (g).

medium moment arm, which can modify the susceptibilities/conductivity and produce remarkable anomalies. Stein et al. (1992, 1994) propose that the fault plane solutions of earthquakes can be employed to depict the distribution of Coulomb failure stress. For simulations of the thrust fault of the Chi-Chi earthquake, Ma et al. (2005) show that the positive Coulomb failure stress forms an ellipse surrounding the fault. Moreover, the belt zone in Fig. 7c can be expressed by a quarter-ring function with SMART as an origin, $38^2 \le Hsf^2 + Hsa^2 \le 62^2$, which is consistent with the distribution of the positive Coulomb failure stress. The agreement of increasing θ_d decreases with Hss between the tendency derived from $38^2 \le Hsf^2 + Hsa^2 \le 62^2$ and the ribbon in Fig. 7e indicates that the appearance of anomalies depends on both Hsf and Hsa.

In conclusion, the scatter distribution of anomalous events in the epicentral system can be transferred into an anomalous belt in the hybrid system. The observation probabilities of anomalous events in the anomalous range of the hybrid system are almost 100% and certainly higher than that of the epicentral system. The hybrid system provides more information and has better performance for identifying anomalous and non-anomalous regions as well as determining the fault plan, the locations of SMART and the occurrence time of earthquakes.

Acknowledgements

The authors wish to thank the guest editor of JSS008, JSS009 and JSS010 (EMSEV) Session at IUGG07 of Tectonophysics, Prof. Pier Francesco Biagi at the Physics Department, University of Bari, Bari, Italy for the invitation of paper submission. This study is partially supported by the project NSC98-2116-M-008-006-MY3 of the National Science Council to the National Central University. The authors thank the Institute of Earth Sciences, Academia Sinica at Taiwan for making the whole dataset behind the analysis of this paper available at ftp://ftp.earth.sinica.edu.tw/pub/Geomagnetic%20Data/ to anyone who is interested in and/or may want to check the results.

References

Bakun, W.H., Aagaard, B., Dost, B., Ellsworth, W.L., Hardebeck, J.L., Harris, R.A., Ji, C., Johnston, M.J.S., Langbein, J., Lienkaemper, J.J., Michael, A.J., Murray, J.R., Nadeau, R. M., Reasenberg, P.A., Reichle, M.S., Roeloffs, E.A., Shakal, A., Simpson, R.W., Waldhauser, F., 2005. Implications for prediction and hazard assessment from the 2004 Parkfield earthquake. Nature 437, 969–974.

Booth, D.C., Crampin, S., Lovell, J.H., Chiu, J.-M., 1990. Temporal changes in shear wave splitting during an earthquake swarm in Arkansas. J. Geophys. Res. 95 (B7), 11151–11164.

Chapman, S., Bartels, J., 1940. Geomagnetism. The Clarendon Press, Oxford. 1049 pp.
Chen, C.S., Chen, C.C., 2000. Magnetotelluric soundings of the source area of the 1999 Chi-Chi earthquake in Taiwan: evidence of fluids at the hypocenter. Terr. Atmo. Ocean Sci. 11, 679–688.
Chen, Y.G., Chen, W.S., Lee, J.C., Lee, Y.H., Lee, C.T., Chang, H.C., Lo, C.H., 2001. Surface rupture of 1999 Chi-Chi earthquake yields insights on active tectonics of central Taiwan. Bull. Seismol. Soc. Am. 91 (5), 977–985.
Chen, C.H., Liu, J.Y., Yen, H.Y., Zeng, X., Yeh, Y.H., 2004. Changes of geomagnetic total field and occurrences of earthquakes in Taiwan. Terr. Atmo. Ocean. Sci. 15, 361–370.
Crampin, S., 1994. The fracture criticality of crustal rocks. Geophys. J. Int. 118, 428–438.
Crampin, S., Volti, T., Stefansson, R., 1999. A successfully stress-forecast earthquake. Geophys. J. Int. 138, F1–F5.
Egbert, G.D., 2002. On the generation of ULF magnetic variations by conductivity fluctuations in a fault zone. Pure Appl. Geophys. 159, 1205–1227.
Engdahl, E.R., van der Hilst, R., Buland, R., 1998. Global teleseismic earthquake relocation with improved travel times and procedures for depth determination. Bull. Seismol. Soc. Am. 88, 722–743.
Fraser-Smith, A.C., Bernardi, A., McGill, P.R., Ladd, M.E., Helliwell, R.A., Villard, O.G., 1990. Low-frequency magnetic field measurements near the epicenter of the Ms 7.1 Loma Prieta earthquake. Geophys. Res. Lett. 17, 1465–1468.
Hattori, K., 2004. ULF Geomagnetic changes associated with large earthquakes. Terr. Atmo. Ocean Sci. 15, 329–360.
Hayakawa, M. (Ed.), 1999. Atmospheric and Ionospheric Electromagnetic Phenomena Associated with Earthquakes. Terra Sci. Pub. Co., Tokyo. 996 pp.
Hayakawa, M., Fujinawa, Y., 1994. Electromagnetic Phenomena Related to Earthquake Prediction. Terra Sci. Pub. Co., Tokyo. 677 pp.
Hayakawa, M., Molchanov, O.A. (Eds.), 2002. Seismo-Electromagnetics: Lithosphere–Atmosphere–Ionosphere Coupling. Terra Sci. Pub. Co., Tokyo. 477 pp.
Johnston, M.J.S., 1997. Review of electric and magnetic fields accompanying seismic and volcanic activity. Surv. Geophys. 18, 441–476.
Kao, H., Liu, Y.H., Liang, W.T., Chen, W.P., 2002. Source parameters of regional earthquake in Taiwan: 1999–2000 including the Chi-Chi earthquake sequence. Terr. Atmo. Ocean Sci. 13, 279–298.
Langbein, J., Borcherdt, R., Dreger, D., Fletcher, J., Hardebeck, J.L., Hellweg, M., Ji, C., Johnston, M., Murray, J.R., Nadeau, R., Rymer, M.J., Treiman, J.A., 2005. Preliminary report on the 28 September 2004, M 6.0 Parkfield, California earthquake. Seismol. Res. Lett. 76, 10–26.
Liang, W.T., Liu, Y.H., Kao, H., 2003. Source parameters of regional earthquake in Taiwan: January–December 2001. Terr. Atmo. Ocean Sci. 14, 249–260.
Liang, W.T., Liu, Y.H., Kao, H., 2004. Source parameters of regional earthquake in Taiwan: January–December 2002. Terr. Atmo. Ocean Sci. 15, 727–741.
Liu, J.Y., Chen, C.H., Chen, Y.I., Yen, H.Y., Hattori, K., Yumoto, K., 2006. Seismo-geomagnetic anomalies and M ≥ 5.0 earthquakes observed in Taiwan during 1988–2001. Phy. Chem. and E. 31, 215–222.
Ma, K.F., Chan, C.H., Stein, R.S., 2005. Response of seismicity to Coulomb stress triggers and shadows of the 1999 Mw = 7.6 Chi-Chi, Taiwan earthquake. J. Geophys. Res. 110, B05S1910.1029/2004JB003389.
Merzer, M., Klemperer, S.L., 1997. Modeling low-frequency magnetic-field precursor to the Loma Prieta earthquake with a precursory increase in fault-zone conductivity. Pure Appl. Geophys. 150, 217–248.
Nagata, T., 1970. Anisotropic magnetic susceptibility of rocks under mechanical stresses. Pure Appl. Geophys. 78, 110–122.
Nishida, Y., Sugisaki, Y., Takahashi, K., Utsugi, M., Oshima, H., 2004. Tectonomagnetic study in the eastern part of Hokkaido, NE Japan: discrepancy between observed and calculated results. Earth Planets Space 56, 1049–1058.
Prasad, S.N., 1999. An inversion of geomagnetic deep sounding data using simulated annealing. Phys. Earth Planet. In. 110, 129–135.
Prasad, S.N., Verma, S.K., Pek, J., Cerv, V., 1993. 2-D inversion of geomagnetic deep sounding data near Ujjain-Guna. India. Geophys. J. intl. 113, 767–775.
Shearer, P.M., 1999. Introduction to Seismology. Cambridge Univ, Press, San Diego. 260 pp.
Stacey, F.D., 1962. Theory of the magnetic susceptibility of stressed rocks. Phil. Mag. 7, 551–556.
Stein, R.S., King, G.C.P., Lin, J., 1992. Change in failure stress on the southern San Andreas fault system caused by the 1992 magnitude = 7.4 Landers earthquake. Science 258, 1328–1332.
Stein, R.S., King, G.C.P., Lin, J., 1994. Stress triggering of the 1994 M = 6.7 Northridge, California, earthquake by its predecessors. Science 265, 1432–1435.
Wang, C., Huang, C.P., Ke, L.Y., Chien, W.J., Hsu, S.K., Shyu, C.T., Cheng, W.B., Lee, C.S., Teng, L.S., 2002. Formation of the Taiwan Island as a solitary wave along the Eurasian continental plate margin: magnetic and seismological evidence. Terr. Atmo. Ocean Sci. 13, 339–354.
Winterstein, D.F., Meadows, M.A., 1991. Shear-wave polarizations and subsurface stress directions at Lost Hills field. Geophysics 56, 1331–1348.
Yen, H.Y., Chen, C.H., Yeh, Y.H., Liu, J.Y., Lin, C.R., Tasi, Y.B., 2004. Geomagnetic fluctuations during the 1999 Chi-Chi earthquake in Taiwan. Earth Planets Space 56, 39–45.
Zeng, X., Liu, J.Y., Lin, Y., Xu, C., 2002. The evolution of dynamic imagines of geomagnetic field and strong earthquake. J. Atmo. Elec. 22, 191–205.